Optics Letters

Tunable and coherent terahertz source based on $CdSiP_2$ crystal via collinear difference frequency generation

Yang Li,[1,2] Jingguo Huang,[1] Zhiming Huang,[1,2,3,6] Guodong Zhang,[4,7] Yanqing Gao,[1] and Yi Shi[5]

[1]State Key Laboratory of Infrared Physics, Shanghai Institute of Technical Physics CAS, Shanghai 200083, China
[2]University of Chinese Academy of Sciences, Beijing 100049, China
[3]Key Laboratory of Space Active Opto-Electronics Technology, Shanghai Institute of Technical Physics CAS, Shanghai 200083, China
[4]State Key Laboratory of Crystal Materials, Shandong University, Jinan 250100, China
[5]College of Science, Donghua University, Shanghai 201620, China
[6]e-mail: zmhuang@mail.sitp.ac.cn
[7]e-mail: zgd@sdu.edu.cn

Received 10 February 2022; revised 16 March 2022; accepted 12 April 2022; posted 13 April 2022; published 2 May 2022

$CdSiP_2$ (CSP) crystals have attracted increasing attention as efficient optical conversion media. Herein, the optical properties of a CSP crystal grown with the vertical Bridgman method are measured by a terahertz time-domain spectrometer (THz-TDS) at 0.2–3 THz. For the first time, to the best of our knowledge, the broadband, tunable, coherent, monochromatic THz radiation from 0.08 to 1.68 THz (3775–178 μm) is generated experimentally via this crystal, which is pumped by a nanosecond Q-switched Nd:YAG laser and an optical parametric oscillator (OPO) and based on difference frequency generation (DFG) technology. The output power and its corresponding conversion efficiency at 0.74 THz are 26.6 mW and 1.4×10^{-7}, respectively. Our work demonstrates that the CSP crystal is a potential efficient terahertz DFG candidate for out-of-door applications.

https://doi.org/10.1364/OL.455950

During the past three decades, the terahertz (THz) frequency located in the range from 0.1 THz to 10 THz has been extensively studied. This special frequency domain has played an important role in material control [1], communication [2], biology [3], imaging [4], security [5], and astronomy [6]. Among them, numerous efforts have been dedicated to develop a THz source. As one of the methods for terahertz wave generation, difference frequency generation (DFG) has the inherent characteristics of wide tuning range, narrow radiation linewidth, relatively high power, and operability at room temperature [7]. Different nonlinear crystals, such as GaSe [8], GaP [9], $LiNbO_3$ [10], GaAs [11], $ZnGeP_2$ (ZGP) [12], DAST [13,14], and BNA [15], have been applied as frequency transfer media in this optical to terahertz conversion technology. Currently, one of the most important things to achieve high-quality terahertz DFG is to pursue higher performance nonlinear crystals as efficient conversion media.

Recently, the $CdSiP_2$ (CSP) crystal has attracted much attention due to the most optimal characteristics of CSP for nonlinear optical conversion. CSP is a tetragonal point group ($\bar{4}2m$), negative uniaxial chalcopyrite crystal in the II-IV-V_2 family. It demonstrates attractive properties including a wide transparent spectral range (0.55–9 μm), pumping at 1.06 μm without two photon absorption, and high laser damage threshold [16–18]. The nonlinear optical coefficient ($d_{36} \sim 84.5$ pm/V) of CSP is larger than the above-mentioned GaSe, GaP, $LiNbO_3$, $ZnGeP_2$, and DAST crystals at 1.06 μm. Two-photon absorption limits the GaAs crystal pumped near 1 μm. The absorption coefficient of $LiNbO_3$ [19], DAST [20], and BNA crystals is larger than that of the CSP crystal at 1–2 THz. Compared with the widely used similar chalcopyrite $ZnGeP_2$ crystals, the wider bandgap, shorter pumped wavelengths (between 1 and 1.5 μm), and lower absorption losses at 2 μm of the CSP crystal make it an attractive alternative to ZGP. However, there are a few theoretical discussions and calculations about terahertz DFG via the CSP crystal [21] and no reported experimental THz generation results.

In this work, we demonstrate the feasibility to realize terahertz generation via DFG by the CSP crystal in experiment for the first time. The broadband, tunable, coherent, monochromatic 0.08–1.68 THz wave is generated by a Q-switched nanosecond pulses Nd:YAG laser source and optical parametric oscillator (OPO) system at near-infrared radiation. It is an important milestone for the CSP crystal to show a great deal of potential practical applications in terahertz DFG technology. We also present a detailed study on the CSP optical properties in the range of 0.2–3 THz. It is the first time that Sellmeier equations are deployed to fit the dispersion of the refractive index.

The time domain spectrum in the terahertz range was obtained via the terahertz time-domain spectrometer (THz-TDS) TeraPulse 4000 (TeraView, Cambridge, UK). The wideband THz emission used in this instrument was generated from photoconductive antennas pumped by a femtosecond fiber laser. The CSP crystal available for this experiment was grown using the vertical Bridgman method. It was a double polished chip cut along the

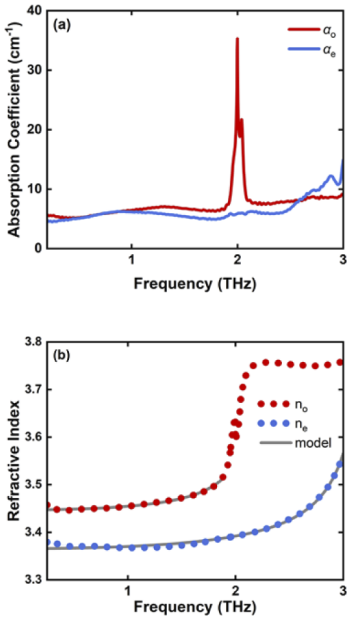

Fig. 1. Optical properties of the CSP crystal in the terahertz range: (a) ordinary α_o and extraordinary α_e absorption coefficients of the CSP crystal; (b) ordinary n_o, extraordinary n_e, and model refractive index of the CSP crystal at room temperature.

<110> plane with 7 mm × 7 mm area and 1.38-mm thickness. The damage threshold was 0.32 J/cm^2. For the CSP crystal, the time domain spectra of the ordinary beam and the extraordinary beam were measured by aligning the optical axis and terahertz wave vector orthogonally or in parallel, respectively. Figures 1(a) and 1(b) present the measured terahertz optical properties of the absorption coefficient and refractive index. One peak absorption of the ordinary beam at 2.0 THz is obviously observed, which theoretically arise from the resonant TO phonon modes [22]. So the refractive index of the n_o is approximated only in the region of 0.2–2.0 THz. The dispersions of n_o and n_e are recorded in this study for the first time to fit Sellmeier equations in the THz region,

$$\begin{aligned} n_o^2 &= 11.65303 + \frac{0.22857\lambda^2}{\lambda^2 - 16947.7}, \lambda\,[\mu m] \in [150, 1500] \\ n_e^2 &= 11.01352 + \frac{0.31341\lambda^2}{\lambda^2 - 8125.5}, \lambda\,[\mu m] \in [100, 1500] \end{aligned} \quad . \quad (1)$$

where λ is in micrometers. Meanwhile, the absorption coefficient of the crystal is quite low, ranging from 5 cm^{-1} to 7 cm^{-1} with frequency located in the 0.2–1.87 THz range.

The schematic diagram of the DFG system with the CSP crystal is illustrated in Fig. 2(a). The fundamental pump source is a Q-switched Nd:YAG laser (Continuum Electro-Optics Inc., USA), providing narrow linewidth pulses (~0.003 cm^{-1}) with pulse duration ~7.8 ns and repetition rate ~10 Hz at 1.0644 μm. The secondary pump source for the DFG is an orthogonal polarized signal from an OPO system, which is pumped by the frequency-tripled (355 nm) emission from the same Nd:YAG laser. This pump beam has the continuously tunable wavelength from 0.4 to 1.7 μm, ~0.075-cm^{-1} linewidth, ~3.8-ns pulse duration, and the same repetition rate (10 Hz). The same pulse energy (1.5 mJ) for the fundamental and OPO signal pump beams are incident on the surface of the CSP crystal.

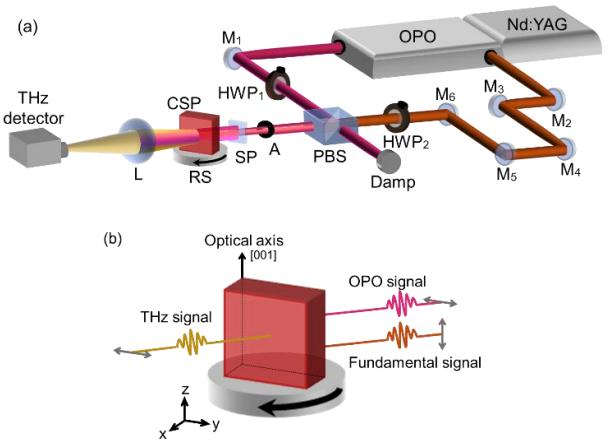

Fig. 2. (a) Schematic of the difference frequency terahertz generation with the CSP crystal; (b) relationship between the crystal rotation direction and polarization of optical waves.

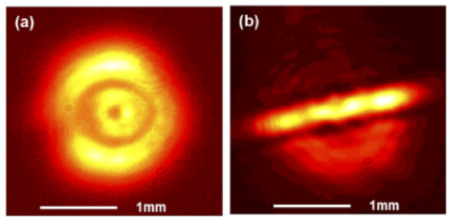

Fig. 3. Laser spot pattern comparison: (a) laser spot pattern before using SP; (b) laser spot pattern after using SP.

The flat mirrors $M_{(1–6)}$ are all highly reflective in the near-infrared band. The $M_{(3–6)}$ mirrors form an optical delay system which ensures that the two pump pulses arrive at the CSP crystal surface at the same time. The attenuator (A) consisting of a half-wave plate $HWP_{(1–2)}$ and a polarized beam splitter (PBS) is used to prevent crystal damage from high laser power. As shown in Fig. 2(b), the crystal is mounted on a two-dimensional horizontal high precision rotation stage (RS). It is assumed that the crystal is at 0 degree position while the pump beam is orthogonal to the crystal input facet (the 7 mm × 7 mm rectangular surface of CSP crystal is regarded as the input facet). The incident fundamental signal and OPO signal are polarized to be parallel and perpendicular to the optical axis of the CSP crystal, respectively. The horizontally polarized THz signal is also observed at the same time. A piece of special plastic (SP) sheet is placed before the CSP crystal, which works like a "cylindrical lens." It is used to shape the circular diffraction pumped spots into an elliptical shape with even energy, as shown in Fig. 3. It improves the optical pump power distribution density, avoiding walk off angles which can hinder terahertz generation. The polyethylene lens (L) is not only used to focus the THz wave, but also prevent the pump beams from transmitting to cause damage to the detector. The generated THz wave is collected by a Schottky-diode terahertz detector (ACST GmbH, Germany). The electrical signal produced by the Schottky-diode THz detector is recorded with a high speed oscilloscope (Teledyne LeCroy Inc., USA).

The CSP crystal has high transmittance in the near-infrared band [23]. Moreover, the birefringence shows sufficient dispersion. For instance, $\Delta n = n_o - n_e \approx 0.05$ at 1.06 μm, so it is almost assumed as an isotropic nonlinear crystal. Figure 4 exhibits the

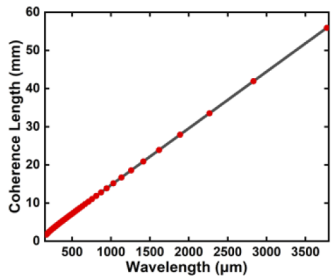

Fig. 4. Coherence length L_c for the CSP crystal versus output THz wavelength.

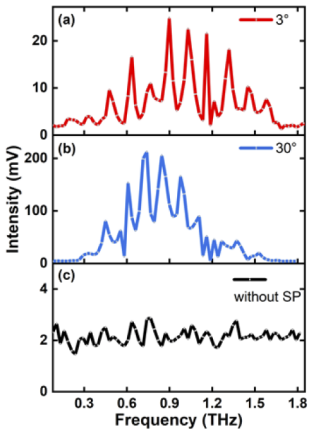

Fig. 5. (a) and (b) THz output voltage when the crystal is tuned at the 3° and 30° positions with an SP sheet, respectively; (c) output voltage at the 30° position, without an SP sheet.

values of the coherence lengths L_c [24] of the CSP crystal versus output THz wavelength, which are calculated using

$$L_c = \frac{\pi}{2}\frac{\lambda_T}{\left(n_P - \frac{\lambda_p}{\lambda_p-\lambda_s}(n_P - n_s) - n_T\right)}, \tag{2}$$

where the wavelength of the fundamental pump signal and OPO signal are λ_p and λ_s, respectively, for difference frequency mixing. In addition, the wavelength of the generated THz signal is λ_T and n_p, n_s, and n_T correspond to the refractive indexes of the pump signal, OPO signal, and output THz signal, respectively. As for the CSP crystal, the minimum coherence length for the DFG process was approximately 1.7 mm, which is a reasonable length that is long enough to generate THz radiation. In conclusion, CSP has been proven to be a promising generator of intense THz radiation.

Figures 5(a) and 5(b) show the measured THz output voltage versus THz frequency when the crystal is tuned at the 3° and 30° positions, respectively, with an SP sheet placed before the crystal. Figure 5(c) shows the output voltage at the 30° position, without an SP sheet. The pump signal wavelength from the OPO system was scanned from 1.0644 μm to 1.0711 μm with a small step resolution of ~0.0001 μm. The corresponding output tunable output terahertz signal was observed from 3775 μm (0.08 THz) to 178 μm (1.68 THz). Comparing the output THz voltages at the 30° position with those at the 3° position, the THz peak voltage (213 mV) at the 30° position is found at 0.74 THz with the OPO signal pulse pumped at ~1.0670 μm, while the THz peak voltage (25 mV) at 3° is located at the 0.89-THz position with the OPO signal pulse pumped at ~1.0676 μm. The THz peak voltage at the 30° position is ~8.5 times larger than that at the 3° position. This results from the inhomogeneity of the crystal quality where both the refractive index and the phase matching relationship are altering with the crystal position. Furthermore, there is an obvious decline for the Schottky-diode terahertz detector in responsivity with the increase of terahertz frequency. The output THz voltages are relatively small and tend to decline because of the responsivity decline at higher terahertz frequency. The regularly distributed diffraction peaks in this figure are attributed to the thickness of the crystal.

Finally, 26.6-mW of THz power is obtained at the observed peak voltage at 0.74 THz, corresponding to the power conversion efficiency of 1.4×10^{-7}. The theoretical THz power and conversion efficiency of the CSP crystal at 0.74 THz is analyzed by calculation using the well-known formula [25], as shown in the following:

$$\frac{P_3}{P_1} = 2\left(\frac{\mu_0}{\varepsilon_0}\right)^{\frac{1}{2}}\frac{\omega_3^2 d_{\text{eff}}^2 L^2}{n_1 n_2 n_3 c^2}\left(\frac{P_2}{A}\right)T_1T_2T_3\exp(-\alpha_3 L) \times \frac{1+\exp(-\Delta\alpha L)-2\exp\left(\frac{-\Delta\alpha L}{2}\right)\cos(\Delta k L)}{(\Delta k L)^2+\left(\frac{\Delta\alpha L}{2}\right)^2}, \tag{3}$$

where μ_0 and ε_0 are the vacuum magnetic permeability and dielectric permittivity, respectively; ω_3 is the output THz frequency; d_{eff} is the effective nonlinear optical coefficient; L is the thickness of the CSP crystal; P_2/A is the input peak intensity of the OPO signal; n_i (i = 1, 2, 3) is the refractive index of the pump signal, OPO signal, and THz signal, respectively; $T_i[T_i = 4n_i/(n_i+1)^2]$ is the relative transmission coefficient; α_i (i = 1, 2, 3) is the absorption coefficient of the pump signal, OPO signal, and THz signal, respectively; $\Delta\alpha = |\alpha_1 + \alpha_2 - \alpha_3|$. Here, $d_{\text{eff}} = 84.5$ pm/V, $L = 1.38$ mm, $P_2/A = 69$ MW/cm^2, $n_1 = 3.11$, $n_2 = 3.16$, $n_3 = 3.40$, $\alpha_1 = \alpha_2 \approx 0.1$ cm^{-1}, $\alpha_3 \approx 5.9$ cm^{-1} at 0.74 THz, and $\Delta k = 0$. The calculated THz power achieved is 28 mW, and the corresponding power conversion efficiency is approximately 1.5×10^{-7}. In conclusion, the theoretical THz power coincides well with the measured result.

In this article, the dispersion equations have been presented for the first time in the THz spectral range based on the measured experimental data at 0.2–2 THz. Furthermore, the broadband, tunable, coherent, monochromatic THz emission has been generated in the CSP crystal using DFG in the range of 0.08–1.68 THz for the first time. The coherence lengths of DFG are long enough for terahertz generation, which is not limited by the phase matching angle. The output THz power and the corresponding conversion efficiency calculated at 0.74 THz are 26.6 mW and 1.4×10^{-7}, respectively. Further, if the CSP crystal quality is improved by increasing the damage threshold, cooling the crystal, and coating the crystal surface in future research, wider tuning range and higher power terahertz sources could be obtained for remote sensing applications. We believe that our results will inspire more researchers to deeply understand the CSP crystal for applications in the terahertz range and attract more research on this high-performance crystal.

Funding. National Science Fund for Distinguished Young Scholars (61625505, 12134016); Chinese Academy of Sciences (ZDBS-LY-JSC025); Sino-Russia International Joint Laboratory of Terahertz Materials and Devices (18590750500); Shanghai Municipal Science and Technology Major Project (2019SHZDZX01).

Acknowledgment. The authors thank Qiu Qinxi and Luo Yunqi for fruitful discussions.

Disclosures. The authors declare no conflicts of interest.

Data availability. Data underlying the results presented in this Letter are not publicly available at this time, but may be obtained from the authors upon reasonable request.

REFERENCES

1. T. Kampfrath, K. Tanaka, and K. A. Nelson, Nat. Photonics **7**, 680 (2013).
2. R. Degl'Innocenti, S. J. Kindness, H. E. Beere, and D. A. Ritchie, Nanophotonics **7**, 127 (2018).
3. R. Zhou, C. Wang, W. Xu, and L. Xie, Nanoscale **11**, 3445 (2019).
4. D. M. Mittleman, Opt. Express **26**, 9417 (2018).
5. A. Ren, A. Zahid, D. Fan, X. Yang, M. A. Imran, A. Alomainy, and Q. H. Abbasi, Trends Food Sci. Technol. **85**, 241 (2019).
6. Y. Kawano, Contemp. Phys. **54**, 143 (2013).
7. K. Zhong, W. Shi, D. Xu, P. Liu, Y. Wang, J. Mei, C. Yan, S. Fu, and J. Yao, Sci. China: Technol. Sci. **60**, 1801 (2017).
8. D. Yan, Y. Wang, D. Xu, P. Liu, C. Yan, J. Shi, H. Liu, Y. He, L. Tang, and J. Feng, Photonics Res. **5**, 82 (2017).
9. T. Tanabe, K. Suto, J. Nishizawa, K. Saito, and T. Kimura, Appl. Phys. Lett. **83**, 237 (2003).
10. T. Akiba, Y. Seki, M. Odagiri, I. Hashino, K. Suizu, Y. H. Avetisyan, K. Miyamoto, and T. Omatsu, Jpn. J. Appl. Phys. **54**, 062202 (2015).
11. T. Nakahama, N. Ozaki, H. Oda, N. Ikeda, and Y. Sugimoto, Jpn. J. Appl. Phys. **59**, 090903 (2020).
12. A. A. Sirotkin, N. N. Yudin, V. V. Dyomin, and A. I. Gribenyukov, Laser Phys. Lett. **17**, 035402 (2020).
13. Y.-X. He, Z.-B. Pang, X.-L. Zhu, D.-G. Xu, Y.-Y. Wang, D.-L. Meng, C. Wu, H.-J. Cheng, Y.-K. Xu, and J.-Q. Yao, J. Infrared and Millimeter Waves **38**, 485 (2019).
14. H. Ito, K. Suizu, T. Yamashita, A. Nawahara, and T. Sato, Jpn. J. Appl. Phys **46**, 7321 (2007).
15. K. Miyamoto, H. Minamide, M. Fujiwara, H. Hashimoto, and H. Ito, Opt. Lett. **33**, 252 (2008).
16. S. A. Bereznaya, Z. V. Korotchenko, S. Y. Sarkisov, I. V. Korolkov, B. M. Kuchumov, A. I. Saprykin, and V. V. Atuchin, Mater. Res. Express **5**, 056204 (2018).
17. G. A. Komandin, S. V. Chuchupal, Y. G. Goncharov, O. E. Porodinkov, I. E. Spektor, K. T. Zawilski, and P. G. Schunemann, Mater. Res. Express **6**, 026204 (2018).
18. K. T. Zawilski, P. G. Schunemann, T. C. Pollak, D. E. Zelmon, N. C. Fernelius, and F. K. Hopkins, J. Cryst. Growth **312**, 1127 (2010).
19. Z.-L. Mao, B.-H. Hou, L. Wang, Y.-M. Sun, G.-Q. Liu, and W. Hao, in *Joint 31st International Conference on Infrared and Millimeter Waves/14th International Conference on Terahertz Electronics* (2006), p. 465.
20. M. Walther, K. Jensby, S. R. Keiding, H. Takahashi, and H. Ito, Opt. Lett. **25**, 911 (2000).
21. C. Bernerd, P. Segonds, J. Debray, J.-F. Roux, E. Herault, J.-L. Coutaz, I. Shoji, H. Minamide, H. Ito, D. Lupinski, K. Zawilski, P. Schunemann, X. Zhang, J. Wang, Z. Hu, and B. Boulanger, Opt. Mater. Express **10**, 561 (2020).
22. Z.-L. Lv, H.-L. Cui, H. Wang, X.-H. Li, and G.-F. Ji, Solid State Commun. **246**, 88 (2016).
23. K. Kato, N. Umemura, and V. Petrov, J. Appl. Phys. **109**, 116104 (2011).
24. J.-Q. Y. B. Sun, B.-G. Zhang, T.-L. Zhang, and P. Wang, Optoelectron. Lett. **3**, 152 (2007).
25. W. Shi, Y. J. Ding, N. Fernelius, and K. Vodopyanov, Opt. Lett. **28**, 136 (2003).